Int J Adv Manuf Technol (2017) 89:2701–2711
DOI 10.1007/s00170-016-9431-5

ORIGINAL ARTICLE

Investigation on chatter stability of thin-walled parts in milling based on process damping with relative transfer functions

Baoguang Liu[1] · **Lida Zhu**[1] · **Yichao Dun**[1] · **Changfu Liu**[1]

Received: 26 July 2016 / Accepted: 31 August 2016 / Published online: 9 September 2016

Abstract Chatter usually occurs in cutting of thin-walled workpiece due to poor structural stiffness, which results in poor surface quality and damaged tool. Aiming at process damping caused by interference between a tool flank face and a machined surface of thin-walled part, the dynamic model and critical condition of stability are proposed by the relative transfer functions, when both the tool structure and the machined workpiece have similar dynamic behaviors in this paper. Using the frequency method to solve the stability of the cutting chatter, it can be seen that the process damping can significantly improve the stability of the low speed region. Moreover, the stability domain is different and more exact than the one that derives from the simple superposition of the tool and the workpiece lobe diagrams. The correctness of the model is validated by experiments. These conclusions provide a theoretical foundation and reference for the milling mechanism research.

Keywords Milling · Process damping · Thin-walled part · Relative transfer functions · Chatter stability

1 Introduction

Thin-walled structural parts play one essential role in aircraft manufacturers. At present, a large number of integral thin-walled structures are used in the aviation industry. And as the aircraft performance requirements continue to improve, the manufacturing level of structural parts of the overall aircraft is also increasing. Peripheral milling of thin-walled part is a common process for aeronautical industry. Multiple experiments proved that thickness is reduced; the rigidity of the parts is reduced, along with the workpiece wall. The machining distortion is increased. Cutting chatter is easy to occur, affecting the machining quality of the parts and causing a reduction in productivity and a reduction of the machine-spindle's working life [1, 2]. As a result of discontinuous cut of milling, the machining process often leads to vibrations of a relative movement between the cutting tool and the workpiece. This movement can lead to the variable chip thickness, which in turn causes a variation of cutting forces. Unstable vibrations is called regenerative chatter, which is a form of self-excited, and can result in undesirable effects on poor surface quality of the workpiece and damaged tool [3–5].

The method of controlling chatter can be generally attributed to the increase of system damping. The damping of cutting system can be divided into the machine structure damping and the process damping of mutual interference between the cutter and the workpiece surface. Analysis and modeling of process damping are hot research fields in recent years. Altintas et al. [6] have presented a cutting force model which has three dynamic cutting force coefficients related to regenerative chip thickness, velocity, and acceleration terms, then the dynamic cutting force coefficient is identified by a large number of dynamic cutting experiments, and the damping coefficient of the process is calibrated. Huang and Wang [7, 8] have extended analytical modeling of the milling process to include process damping effects. In their model, two cutting mechanisms (shearing and plowing) and two process damping effects (direction and magnitude) are included. On the basis of this, Wan et al. [9, 10] made a further research. In his study, plowing mechanism was separately treated for static and dynamic cutting processes. Whether for static or dynamic cutting

✉ Lida Zhu
zld1999@gmail.com

[1] School of Mechanical Engineering and Automation, Northeastern University, Shenyang 110819, China

processes, a unified proportional form is used to express plowing forces as function of the volume of the materials extruded under the clearance face of the tool. The shear force coefficient and the plow force coefficient are calibrated, respectively.

Ahmadi and Ismail [11] have proposed that finite amplitude stability due to process damping in milling is investigated experimentally and numerically. In addition, an amplitude-dependent formulation of process damping is integrated into the semi-discretization method of computing stability lobes to determine the borders of finite amplitude stability region. Budak and Tunc [12–14] have considered the effect of process damping as an additional damper in the zero order MFS. They identified the additional damping coefficients by measuring stability limits experimentally and fitting the results to the stability model and studied the effects of tool geometry and cutting conditions on process damping. Jaydeep et al. [15] have proposed a value of an information-based experimental design method that uses Bayesian inference for belief updating. The application is process damping coefficient identification in milling. An analytical process damping algorithm is used to model the prior distribution of the stability boundary. Ahmadi et al. [16, 17] have presented the equivalent viscous model of process damping is integrated into the multi-frequency solution and the semi-discretization method to establish the stability lobes in milling. Dilley et al. [18] have shown that the compressed volume can be described by a short-delay model. In the governing equation, this contact force is represented by a piecewise constant velocity-dependent damping matrix. Jin and Altintas [19] have proposed the prediction of cutting forces and chatter stability of micro-milling operations from the material's constitutive flow stress and structural dynamics of the micro-end mill. The cutting force coefficients are identified either using the previously presented slip-line field or finite element methods. Moradi et al. [20, 21] have presented an extended dynamic model of peripheral milling process including process damping and structural and cutting force nonlinearities. Cutting forces are described through a third-order polynomial function of chip thickness while a cubic nonlinear function is considered for the structural stiffness. Ahmadi and Altintas [22] have presented a new method in predicting the material-dependent process damping coefficient from chatter-free orthogonal cutting tests. An equivalent process damping coefficient of the dynamic system is estimated from the frequency domain decomposition (FDD) of the vibration signals measured during stable cutting tests.

For the current process damping models, few of these models consider this situation where the cutter subsystem and the workpiece subsystem present similar dynamic behaviors. In this paper, the chatter stability of thin-walled parts based on process damping is studied by the relative movement between the two mechanical systems in contact with each other.

This paper is divided into four main sections, the first section, entitled "The proposed model," proposes a new milling dynamic model of thin-walled workpiece considering process damping and discusses transfer function of thin-walled part and cutter, respectively. The second, a machining stability model considering process damping based on the relative transfer function is established. The third part, the model test was conducted and measurement of milling force coefficient. Experimental verifications and time domain simulation for some different conditions are given in the fourth section. Finally, some conclusions from this study are obtained.

Nomenclature

$h_j(t)$ dynamic chip thickness	$V(t)$ instantaneous indentation volume
$\phi_j(t)$ instantaneous angular immersion of tooth j	K_{sp} Indentation coefficient
$x_t(t)$ dynamic displacement of tool in x direction	S the cross-sectional area
$y_t(t)$ dynamic displacement of tool in y direction	C_{eq} process damping coefficient
$x_w(t)$ dynamic displacement of workpiece in x direction	C_d shape damping coefficient
$y_w(t)$ dynamic displacement of workpiece in y direction	K_t tangential cutting force coefficient
N number of cutter	K_r radial cutting force coefficient
Ω rotational speed of spindle	v cutting speed
$g(\phi_j)$ unit step function	$F_{(j,\phi_j(t))}^{tp}$ plowing forces in radial direction
ϕ_{st} entry angle of side cutting edge	$F_{(j,\phi_j(t))}^{tp}$ plowing forces in radial direction
ϕ_{ex} exit angle of end cutting edge	μ coefficient of friction
$F_{(j,\phi_{j(t)})}^{ts}$ shear forces in tangential direction	k_c stiffness of cutter
$F_{(j,\phi_{j(t)})}^{rs}$ shear forces in radial direction	ζ damp ratio
b axial depth of the cut	m_c modal mass (kg) of cutter
ξ_c^p damp ratio including process damping	C_c structure damping of cutter
k_w modal stiffness (N/mm^2) of workpiece	m_w modal mass (kg) of workpiece
ξ_w^p damp ratio including process damping of workpiece.	C_w structure damping of workpiece
F_0 amplitude of dynamic milling force.	Λ_R real part of the characteristic root
Λ_I imaginary part of the characteristic root	T rotation period of spindle

2 The proposed model

2.1 Model of process damping

With regard to thin-walled workpiece, such as shell and other auto parts, the stability of the machining system is not only influenced by the suspension of the milling cutter but also closely related to the dynamic characteristics of the tool and the workpiece. The model considering the process damping is simplified into two degrees of freedom of the mutual vertical elastic damping system of thin-walled workpiece as shown in Fig. 1, which is based on the double effects of shear force and plowing force which are caused by interference between a tool flank face and a machined surface of the workpiece.

In descriptions of regenerative chatter in machining, dynamic components are caused by the vibrations of the tool at the present and previous tooth periods. Since the chip thickness is measured in the radial direction, the general dynamic chip thickness can be expressed as follows:

$$h_{\mathrm{j}}(t) = \begin{bmatrix} sin\left(\phi_{\mathrm{j}}(t)\right) \\ cos\left(\phi_{\mathrm{j}}(t)\right) \end{bmatrix}^{T} \begin{Bmatrix} \Delta x_{\mathrm{c}} - \Delta x_{\mathrm{w}} \\ \Delta y_{\mathrm{c}} - \Delta y_{\mathrm{w}} \end{Bmatrix} \tag{1}$$

Relative displacement of the tool and workpiece is shown:

$$\begin{Bmatrix} \Delta x_{\mathrm{c}} - \Delta x_{\mathrm{w}} \\ \Delta y_{\mathrm{c}} - \Delta y_{\mathrm{w}} \end{Bmatrix} = \begin{Bmatrix} \left[x_t(t) - x_t(t-T)\right] - \left[x_{\mathrm{w}}(t) - x_{\mathrm{w}}(t-T)\right] \\ \left[y_t(t) - y_t(t-T)\right] - \left[y_{\mathrm{w}}(t) - y_{\mathrm{w}}(t-T)\right] \end{Bmatrix} \tag{2}$$

where $[x_t(t), y_t(t)]^T$ is the dynamic displacement vector of the tool at the present time t. $[x_{\mathrm{w}}(t), y_{\mathrm{w}}(t)]^T$ is the displacement vector of the workpiece at the present time t.

The instantaneous angular immersion of tooth j is the following:

$$\phi_{\mathrm{j}}(t) = (2\pi\Omega/60)t - (j-1)\cdot 2\pi/N \tag{3}$$

where N is the number of cutter, Ω is the rotational speed.

The function $g(\phi_{\mathrm{j}})$ is a unit step function that determines whether the tooth is in or out of cut, that is,

$$g\left(\phi_{\mathrm{j}}(t)\right) = \begin{cases} 1 & \phi_{\mathrm{st}} < \phi_{\mathrm{j}}(t) < \phi_{\mathrm{ex}} \\ 0 & \text{otherwise} \end{cases} \tag{4}$$

where ϕ_{st} and ϕ_{ex} are the start and exit immersion angles of the cutter, respectively.

The shear forces in tangential ($F^{\mathrm{ts}}_{(\mathrm{j},\phi_{\mathrm{j}(t)})}$) and radial direction ($F^{\mathrm{rs}}_{(\mathrm{j},\phi_{\mathrm{j}(t)})}$) acting on the tooth j are proportional to the axial depth of the cut (b) and chip thickness (h):

$$F^{\mathrm{ts}}_{(\mathrm{j},\phi_{\mathrm{j}(t)})} = K_t b h_{(\mathrm{j},\phi_{\mathrm{j}(t)})}, \quad F^{\mathrm{rs}}_{(\mathrm{j},\phi_{\mathrm{j}(t)})} = K_r F^{\mathrm{ts}}_{(\mathrm{j},\phi_{\mathrm{j}(t)})} \tag{5}$$

where K_t and K_r are cutting coefficients.

The plowing force, causing the phenomenon of process damping, is calculated using the indentation model, where the radial plowing force is assumed to be proportional to the instantaneous indentation volumeV(t) of the material extruded underneath the flank face:

$$F^{\mathrm{rp}}_{(\mathrm{j},\phi_{\mathrm{j}}(t))} = g\left(\phi_{\mathrm{j}}(t)\right) K_{\mathrm{sp}} V_{(\mathrm{j},\phi_{\mathrm{j}}(t))}, \quad V_{(\mathrm{j},\phi_{\mathrm{j}}(t))} = bS_{(\mathrm{j},\phi_{\mathrm{j}}(t))} \tag{6}$$

where indentation coefficient K_{sp} in end milling is identified. S is the cross-sectional area between a tool flank face and a machined surface of a part [16].

The plowing force in the tangential direction is presented as follows:

$$F^{\mathrm{tp}}_{(\mathrm{j},\phi_{\mathrm{j}}(t))} = \mu d F^{\mathrm{rp}}_{(\mathrm{j},\phi_{\mathrm{j}}(t))} \tag{7}$$

In order to identify the process damping coefficients in r and u directions, the proposed approach, developed by K. Ahmadi and F. Ismail [17], is applied where μ is the coefficient of friction.

The nonlinear damping is equivalent to linear damping system by the energy equivalence principle. Dynamic displacements of tool vibration are assumed as $r(t)$ and $u(t)$, respectively. Therefore, the process damping force, that is plowing force, can be expressed in orthogonal directions as follows:

$$F^{\mathrm{rp}}_{(\mathrm{j},\phi_{\mathrm{j}}(t))} = C^{\mathrm{r}}_{\mathrm{eq}}\, \dot{r}\,(t), \quad F^{\mathrm{tp}}_{(\mathrm{j},\phi_{\mathrm{j}}(t))} = C^{\mathrm{t}}_{\mathrm{eq}}\, \dot{u}\,(t) \tag{8}$$

$$C^{r}_{eq} = \frac{K_{\mathrm{sp}} b C^{\mathrm{r}}_{\mathrm{d}}}{v}, \quad C^{\mathrm{t}}_{\mathrm{eq}} = \frac{K_{\mathrm{sp}} b C^{\mathrm{t}}_{\mathrm{d}}}{v} \tag{9}$$

where the process damping equivalent coefficients in two directions can be expressed as a function of cutting speed (v) and chip width (b), and C_{d} is designated as the shape damping coefficient. It is difficult to calculate the value of C_{d} in theory. So K. Ahmadi gives a data base of C_{d} through a lot of experiments [16].

Therefore, the total forces including tangential ($F^{\mathrm{t}}_{(\mathrm{j},\phi_{\mathrm{j}(t)})}$) and radial direction ($F^{\mathrm{r}}_{(\mathrm{j},\phi_{\mathrm{j}(t)})}$) acting on the tooth j are shown:

$$F^{\mathrm{t}}_{(\mathrm{j},\phi_{\mathrm{j}(t)})} = F^{\mathrm{ts}}_{(\mathrm{j},\phi_{\mathrm{j}(t)})} + F^{\mathrm{tp}}_{(\mathrm{j},\phi_{\mathrm{j}(t)})} \tag{10}$$

$$F^{\mathrm{r}}_{(\mathrm{j},\phi_{\mathrm{j}(t)})} = F^{\mathrm{rs}}_{(\mathrm{j},\phi_{\mathrm{j}(t)})} + F^{\mathrm{rp}}_{(\mathrm{j},\phi_{\mathrm{j}(t)})} \tag{11}$$

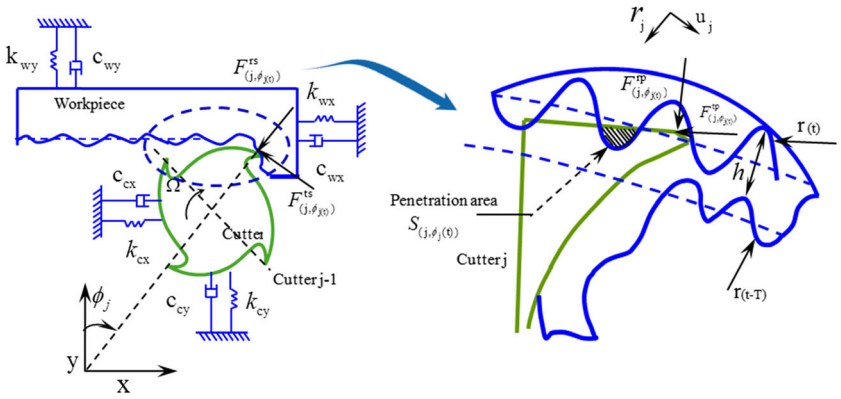

Fig. 1 Two degrees of freedom of the milling system

Then the total forces are transformed from the end mill rotating coordinate system in orthogonal (r) and (u) directions to workpiece coordinate with feed (x) and normal (y) directions.

$$\begin{bmatrix} F^{x}_{(\mathrm{j},\phi_{\mathrm{j}(t)})} \\ F^{y}_{(\mathrm{j},\phi_{\mathrm{j}(t)})} \end{bmatrix} = \begin{bmatrix} -\cos\phi_{\mathrm{j}}(t) & -\sin\phi_{\mathrm{j}}(t) \\ \sin\phi_{\mathrm{j}}(t) & -\cos\phi_{\mathrm{j}}(t) \end{bmatrix} \begin{bmatrix} F^{\mathrm{t}}_{(\mathrm{j},\phi_{\mathrm{j}(t)})} \\ F^{r}_{(\mathrm{j},\phi_{\mathrm{j}(t)})} \end{bmatrix} \tag{12}$$

The cutting forces acting on all the cutter teeth are added together to obtain the total cutting force acting on the whole cutting tool.

$$F^{\mathrm{x}}_{(t)} = \sum_{\mathrm{j}=1}^{N-1} F^{\mathrm{x}}_{\left(\mathrm{j},\phi_{\mathrm{j}(t)}\right)} \quad F^{\mathrm{y}}_{(t)} = \sum_{\mathrm{j}=1}^{N-1} F^{\mathrm{y}}_{\left(\mathrm{j},\phi_{\mathrm{j}(t)}\right)} \tag{13}$$

where $\phi_{\mathrm{j}} = \phi + \phi_p$, Cutter angle $\phi_{\mathrm{p}} = 2\pi/N$. The dynamic cutting thickness expressions (1) and cutting forces (12) are substituted into the formula (13). It is expressed as follows:

$$\begin{Bmatrix} F^{\mathrm{x}}_{(t)} \\ F^{\mathrm{y}}_{(t)} \end{Bmatrix} = \frac{1}{2} b K_t \mathrm{A}_0 \begin{Bmatrix} \Delta x_{\mathrm{c}} - \Delta x_w \\ \Delta y_{\mathrm{c}} - \Delta y_w \end{Bmatrix} \tag{14}$$

where axial cutting depth is represented as b and average milling force direction coefficient matrix is represented by A_0.

2.2 Relative transfer function model

The frequency response function is expressed for the workpiece-tool system in one degree of freedom:

$$\Phi(s) = \frac{y(s)}{F_f(s)} = \frac{\omega_n^2}{k\left(s^2 + 2\xi\omega_n s + \omega_n^2\right)} \tag{15}$$

where k is the stiffness (N/mm^2), ξ is the damp ratio, and ω is the frequency (Hz).

The frequency response function is expressed for the tool subsystem in multi-degrees of freedom as follows:

$$[\Phi(s)]_c = \sum_{k=1}^{n} \frac{a_k^c + \beta_k^c s}{s^2 + 2\xi_k^c \omega_{n,k} + \omega_{n,k}^2} = \sum_{k=1}^{n} \frac{[R]_k^c}{s^2 + 2\xi_k^c \omega_{n,k} + \omega_{n,k}^2} \tag{16}$$

Similarly, the workpiece subsystem frequency response function is given:

$$[\Phi(s)]_w = \sum_{k=1}^{n} \frac{a_k^w + \beta_k^w s}{s^2 + 2\xi_k^w \omega_{n,k} + \omega_{n,k}^2} = \sum_{k=1}^{n} \frac{[R]_k^w}{s^2 + 2\xi_k^w \omega_{n,k} + \omega_{n,k}^2} \tag{17}$$

The two subsystems of tool and workpiece must be studied on the transfer function in the same direction, so two directions transfer functions are established in a space coordinate system. The transfer functions of the tool are expressed in x and y directions as follows:

$$\begin{cases} \Phi_{xx.c}(\omega) = G_{xx.c}(\omega) + jH_{xx.c}(\omega) = \dfrac{\delta_{xx.c}}{F_{xx.c}} \\ \Phi_{yy.c}(\omega) = G_{yy.c}(\omega) + jH_{yy.c}(\omega) = \dfrac{\delta_{yy.c}}{F_{yy.c}} \end{cases} \tag{18}$$

where $G_{\mathrm{c}}(\omega)$ and $H_{\mathrm{c}}(\omega)$ are respectively the real and imaginary parts of the system transfer function of the tool in x and y directions. δ_{c} is the displaced direction of the tool subsystem. F_{c} is the force direction of the tool subsystem.

The transfer functions of the workpiece in x and y directions are as follows:

$$\begin{cases} \Phi_{xx.w}(\omega) = G_{xx.w}(\omega) + jH_{xx.w}(\omega) = \dfrac{\delta_{xx.w}}{F_{xx.w}} \\ \Phi_{yy.w}(\omega) = G_{yy.w}(\omega) + jH_{yy.w}(\omega) = \dfrac{\delta_{yy.w}}{F_{yy.w}} \end{cases} \tag{19}$$

where $G_{\mathrm{w}}(\omega)$ and $H_{\mathrm{w}}(\omega)$ are respectively the real and imaginary parts of the system transfer function of the workpiece in x and y directions. δ_{w} is the displaced direction of the workpiece subsystem. F_{w} is the force direction of the workpiece subsystem.

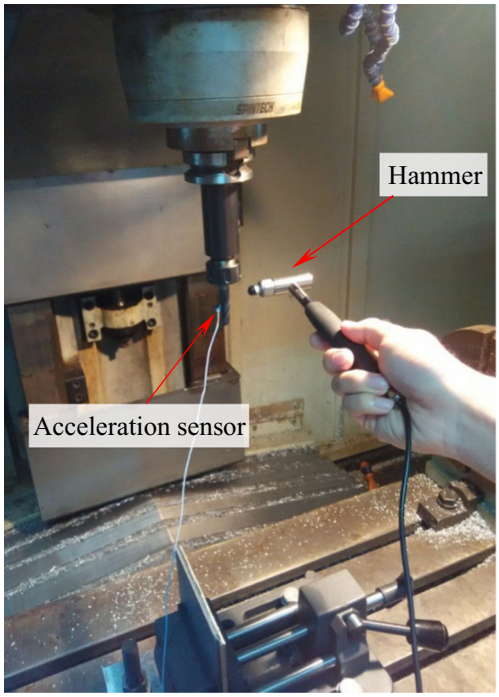

Fig. 2 The cutter modal test

For the tool subsystem and workpiece subsystem, the force values are the same and the force directions is opposite interaction. After the analysis of the transfer function, the forces in x and y directions are expressed as follows:

$$\begin{cases} F_{xx} = |F_{xx.c}| = |-F_{xx.w}| \\ F_{yy} = |F_{yy.c}| = |-F_{yy.w}| \end{cases} \tag{20}$$

The relative movement of the tool subsystem and workpiece subsystem is the addition of displacements in x and y directions, so the two subsystems move away from each other due to the action of the cutting force. The absolute displacements are given as follows:

$$\begin{cases} \delta_{\text{relative}(xx)} = \delta_{c(xx)} + \delta_{w(xx)} \\ \delta_{\text{relative}(yy)} = \delta_{c(yy)} + \delta_{w(yy)} \end{cases} \tag{21}$$

The relative transfer functions between the tool and the workpiece are obtained from Eq. (18)–(21) and analyzed as:

$$\begin{cases} \Phi_{\text{relative}(xx)} = \Phi_{c(xx)} + \Phi_{w(xx)} \\ \Phi_{\text{relative}(yy)} = \Phi_{c(yy)} + \Phi_{w(yy)} \end{cases} \tag{22}$$

It can be noticed that the components of the relative frequency response function (FRF) are the addition between the tool's FRF and the FRF of the workpiece in x and y directions. The resulting FRF will be used for the calculation of the lobe diagram.

3 Chatter stability model based on process damping

The chatter frequency assumed for the milling of thin-walled parts is ω_n. The vibration displacement caused by ω_n is expressed in the frequency domain by using the harmonic function [23, 24].

$$\Delta u_{(t)} = [1-\exp(-i\omega_n T)\Phi^p(i\omega_n)]F_0\exp(i\omega_n t) \tag{23}$$

where $\Delta u_{(t)} = \{\Delta x_c - \Delta x_w \;\; \Delta y_c - \Delta y_w\}$,

$$\Phi^p(i\omega_n) = \Phi_c^p(i\omega_n) + \Phi_w^p(i\omega_n) \tag{24}$$

$\Phi^p(i\omega_n)$ is the transfer function matrix of milling system including process damping; $\Phi_c^p(i\omega_n)$ is the transfer function matrix of cutter subsystem including process damping, which is expressed in one degree of freedom; and F_0 is the amplitude of dynamic milling force.

$$\Phi_c^p(i\omega) = \frac{y(i\omega)}{F(i\omega)} = \frac{\omega_n^2}{k_c\left[(i\omega)^2 + 2\xi_c{}^p\omega_n(i\omega) + \omega_n^2\right]} \tag{25}$$

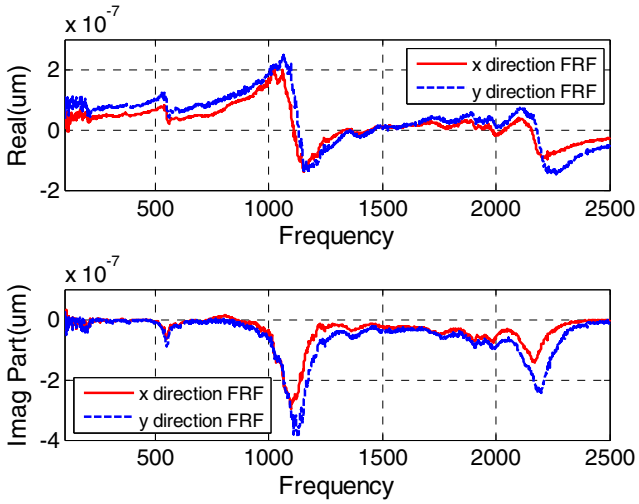

Fig. 3 Two orthogonal direction FRFs measured at the tool tip

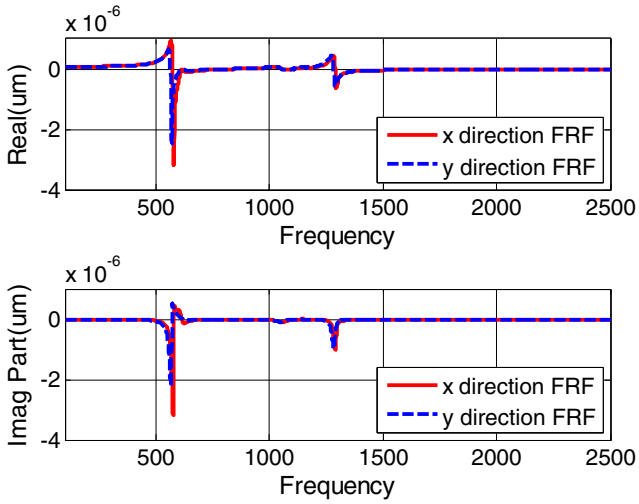

Fig. 4 Two orthogonal direction FRFs measured at the workpiece

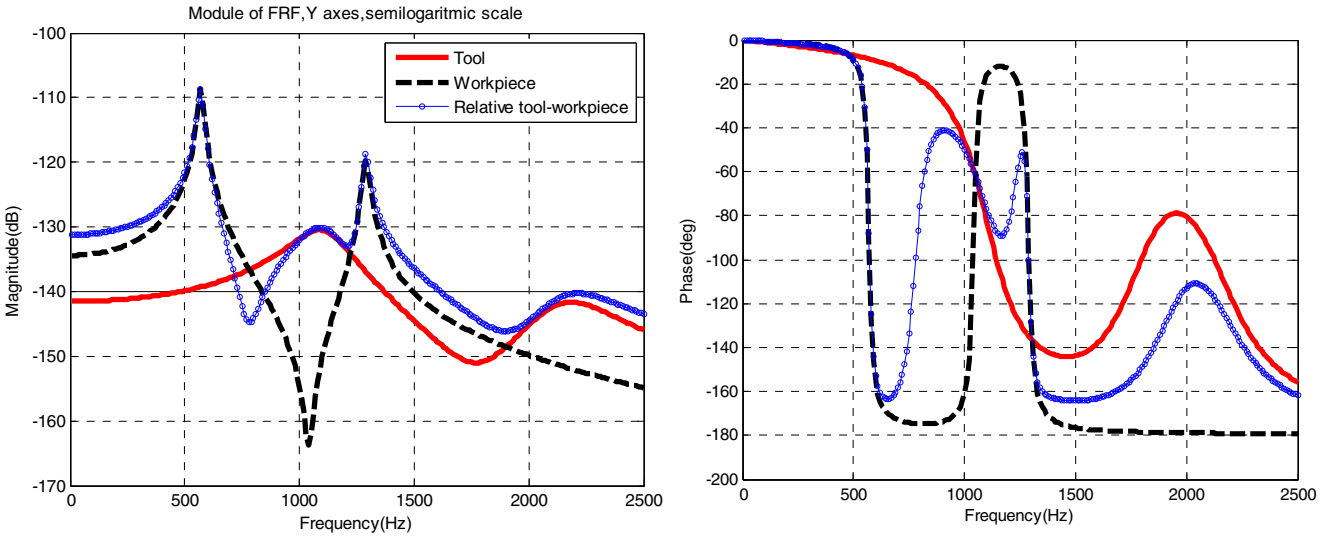

Fig. 5 Comparison of FFT in the *x*-axis, tool, workpiece, and relative. They are semi-logarithmic representations

where ω is the frequency (Hz), k_c is the modal stiffness (N/mm^2) of the cutter, m_c is the modal mass (kg) of cutter, and $\xi_c^{\,p}$ is the damp ratio including process damping.

$$\xi_c^{\,p} = \frac{C_c + C_{eq}}{2\sqrt{k_c m_c}} \tag{26}$$

where C_c is the structure damping of the cutter, C_{eq} is the equivalent process damping of the milling system, and $\Phi_w^p(i\omega_c)$ is the transfer function matrix of the workpiece subsystem including process damping, similarly.

$$\Phi_w^p(i\omega) = \frac{y(i\omega)}{F(i\omega)} = \frac{\omega_n^2}{k_w\left[(i\omega)^2 + 2\xi_w{}^p\omega_n(i\omega) + \omega_n^2\right]} \tag{27}$$

where k_w is the modal stiffness (N/mm^2) of the workpiece, m_w is the modal mass (kg) of the workpiece, and $\xi_w^{\,p}$ is the damp ratio including process damping.

$$\xi_w^{\,p} = \frac{C_w + C_{eq}}{2\sqrt{k_w m_w}} \tag{28}$$

where C_w is the structure damping of the workpiece.

The characteristic equation of the system is obtained as follows:

$$\left| I - \frac{N}{4\pi} bK_t(1-\exp(-i\omega_n T)[\Phi_0{}^p(i\omega_n)] \right| = 0 \tag{29}$$

where transfer function ($\Phi_0{}^p(i\omega_n)$) incorporating directional factor matrix includes process damping.

$$[\Phi_0{}^p(i\omega_n)] = \frac{2\pi A_0}{N}\Phi^p(i\omega_n) \tag{30}$$

Therefore, the characteristic value of the system is the following:

$$\Lambda = -\frac{N}{4\pi} bK_t(1-\exp(-i\omega_n T) = \Lambda_R + i\Lambda_I \tag{31}$$

where Λ_R and Λ_I are the real part and imaginary part of the characteristic root, respectively.

Obtained by formula (21), Λ_R <0, the limit of the critical stability of axial depth is shown:

$$b_{lim}^p = -\frac{2\pi\Lambda_R}{NK_t}\left[1 + \left(\frac{\Lambda_I}{\Lambda_R}\right)^2\right] \tag{32}$$

Table 1 The modal parameters of the tool

Modal parameter	*x* direction			*y* direction		
	Natural frequency (Hz)	Damping ratio	Rigidity (N/m)	Natural frequency (Hz)	Damping ratio	Rigidity (N/m)
First order of cutter	1110	0.1198	1.43e7	1130	0.10	1.31e7
Second order of cutter	2158	0.094	7.8e7	2179	0.063	3.37e7

corresponding speed range:

$$n = \frac{60\omega}{N}\frac{1}{(2k+1)\pi + 2\Psi} \quad k = 0, 1, \ldots \tag{33}$$

where $\Psi = \arctan\frac{\mathrm{Im}[\Phi^{\mathrm{p}}(i\omega)]}{\mathrm{Re}[\Phi^{\mathrm{p}}(i\omega_{\mathrm{n}})]}$.

4 Modal tests and identification of cutting force coefficients

4.1 Modal tests

Hammer mode test is conducted in the TH5650 vertical machining center of Shenyang machine production. As shown in Fig. 2, the main equipment of this experiment is the following: (1) impact hammer (B&K8206-002), sensitivity (0.23 mV/N), the maximum impact force was 22kN; (2) cutting tool is carbide ball end milling cutter, whose diameter is 10 mm; (3) acceleration sensor style 3225F1 (sensitivity 10.00mv/g); (4) dynamic signal acquisition system (Cutpro) and computer; sampling rate (Hz) 50,000, frequency range (Hz) 50–5000, transfer functions: displacement force.

The frequency response functions (real part and imagine part) of the tool point have been measured in x and y directions, as shown in Fig. 3. The frequency response functions (real part and imagine part) of the thin-walled part have been measured in x and y directions, as shown in Fig. 4. The multi-mode relative transfer function of the tool and workpiece (amplitude and phase) in the x direction is shown in Fig. 5.

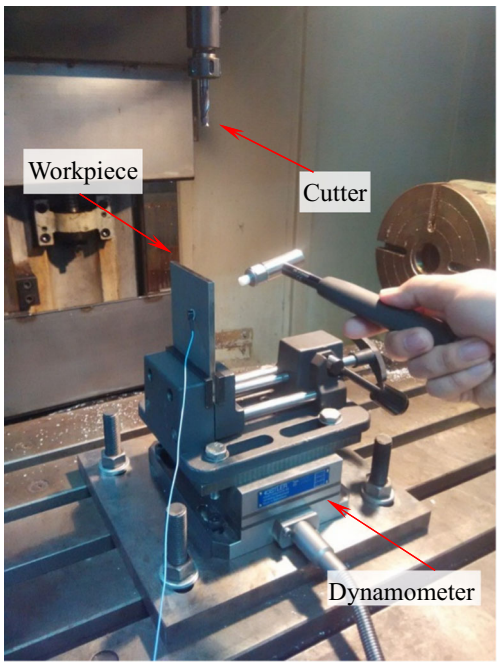

Fig. 6 Measuring cutting force

Table 2 The cutting text data

Test ID	Spindle speed (rpm)	Feed per tooth (mm/z)	Depth of cut (mm)	F_x	F_y	F_z
1	1200	0.04	1	−84.8	126.5	26.37
2	1200	0.06	1	−118.6	104.1	65.64
3	1200	0.08	1	−137	181.8	92.53
4	1200	0.04	2	−100.3	234.2	168.1
5	1200	0.06	2	−62.4	89.7	125.02
6	1200	0.08	2	−46.8	384.3	68.63
7	1200	0.04	3	0.89	403.2	−11.34
8	1200	0.06	3	61.21	520	−64.73
9	1200	0.08	3	68.45	642.1	−117.5

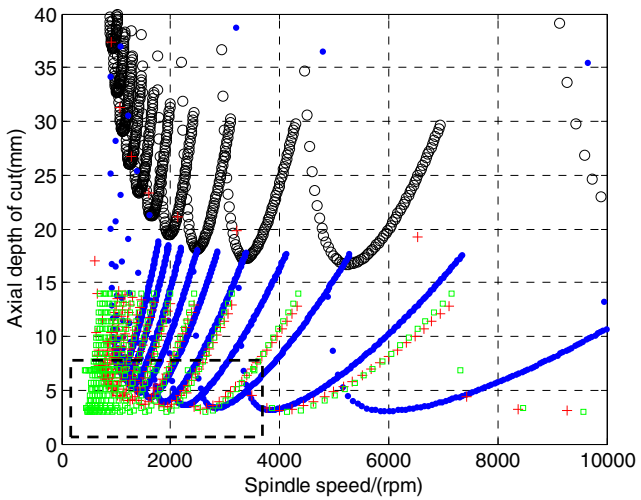

(a) The chatter lobes in the Fig. 7, from 0 to 10000rpm

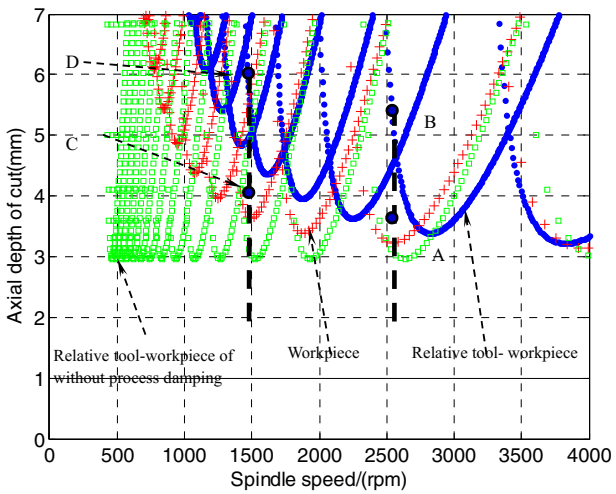

(b) The chatter lobes in the Fig. 7, from 0 to 4000rpm

Fig. 7 Comparison of chatter lobe tool, workpiece, relative, and relative of without process damping. The chatter lobes **a** from 0 to 10,000 rpm and **b** from 0 to 4000 rpm

The FRF matrix of the machine-tool structure at the tool tip (tip-tip FRFs) was determined by an impact test procedure. In order to check for the presence of mode coupling, the tool response was measured in x and y directions at both locations. The measured FRFs were curved fit by commercial modal analysis software to identify the modal parameters and calculate the tip-tip FRFs. The obtained diagonal elements of the system for the tip-tip FRFs are listed in Table 1.

The difference between the transfer function of the relative movement with respect to the treatment of the tool's and workpiece's transfer functions as two independent entities seems obvious, as shown in Fig. 5. The transfer function of the structure of the processing system depends on the relative relationship, calculated with the proposed method, between the tool and workpiece subsystems.

4.2 Identification of cutting force coefficients

The cutting force coefficient of the machining process is identified by the average coefficient milling force model. The experiment was carried out on the TH5650 vertical milling center of Shenyang machine. The tool which has a two-flute cutter with 10 mm diameter, clearance angle (10 deg), has been selected and mounted with 45-mm overhang on an HSK32ER20 tool-holder. The material used for the machining tests was Ti-6Al-4V (TC4) alloy. The size of the workpiece is 5 mm × 100 mm × 100 mm. A three-component Kistler dynamometer type 9257B has been mounted on the machine table, and the coordinate system has been set to level with the force sensor surfaces. The setup of the machining experiment is shown in Fig. 6.

In this experiment, the cutting tool is a carbide alloy material of the ball end mill; the milling cutter helix angle is 30°. Milling parameters are as follows: spindle speed 1200 rpm, each tooth feed [0.04, 0.06, 0.08] mm/z, and axial cutting deep [1, 2, 3] mm. Multi-group experiments were carried out, and the experimental data are shown in Table 2.

By analyzing the relationship of cutting force, the cutting coefficients obtained k_{tc}, k_{rc}, and k_{ac} are 1596.3, 474.5, and 598.7 Mpa by the shearing action in tangential, radial, and axial direction, respectively. And the edge constants k_{te}, k_{re}, and k_{ac} are 30.7, 46.4, and 8.3, respectively. Radial cutting depth is 1 mm, down milling.

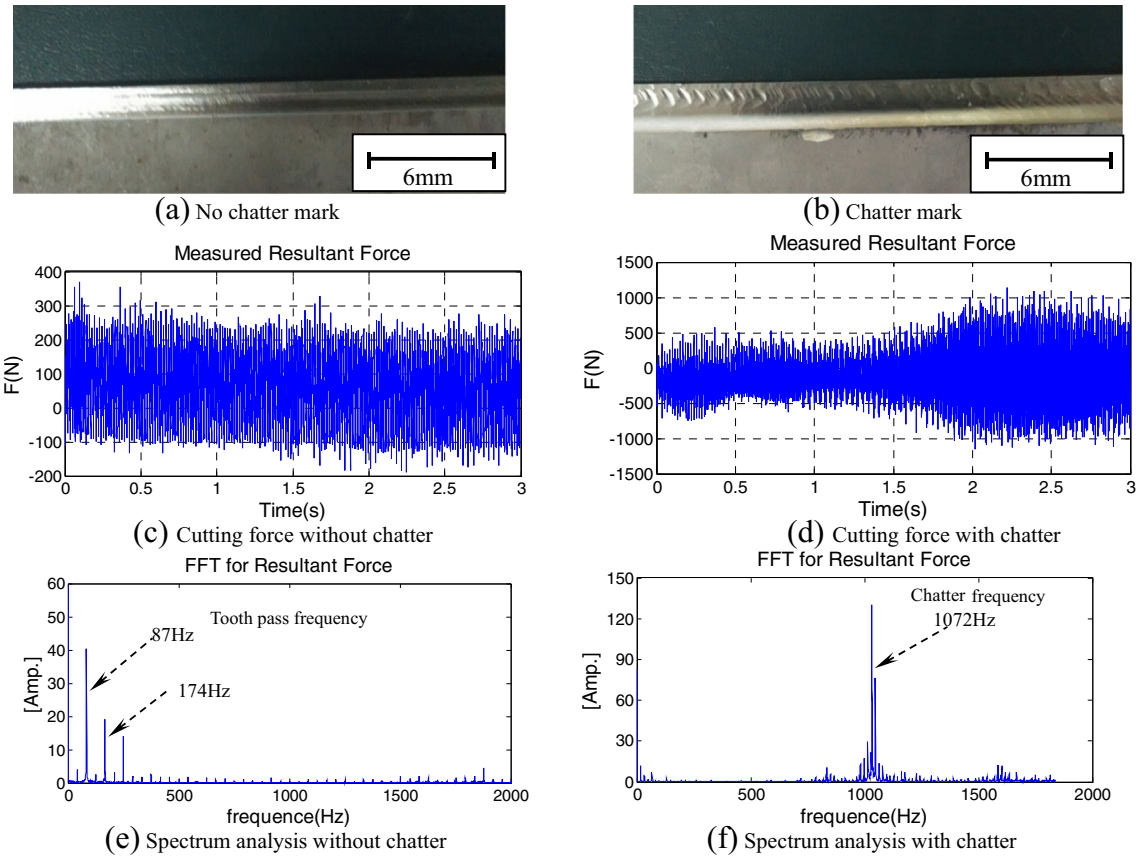

Fig. 8 Analysis results of milling. **a** No chatter mark, **b** chatter mark, **c** cutting force without chatter, **d** cutting force with chatter, **e** spectrum analysis without chatter, and **f** spectrum analysis with chatter

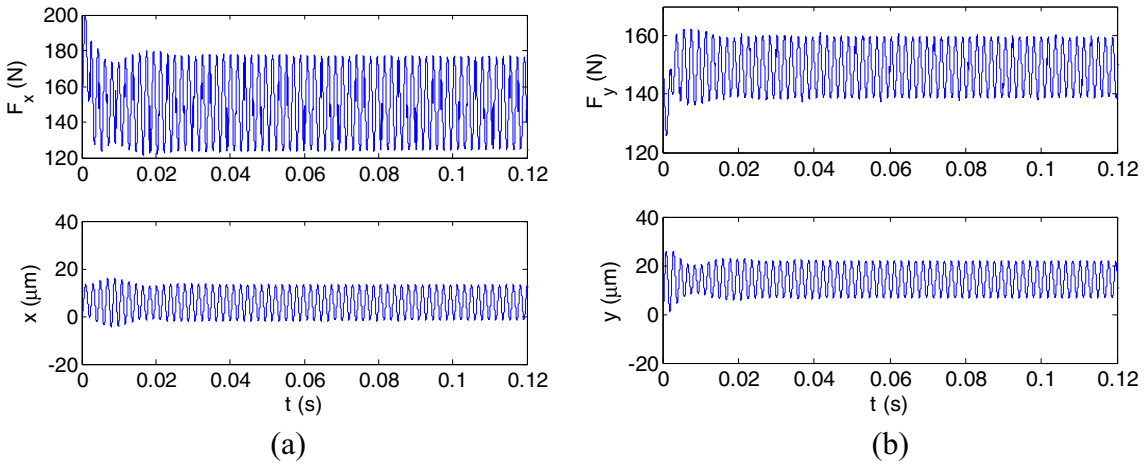

Fig. 9 The *x* and *y* directions of force and displacement of C simulation of the stable point

5 Verification of model predictions

The example case is defined by the following cutting parameters:

- Radial depth of cut is 2 mm, down milling, with a 10 mm diameter carbide tool, 80 mm overall length, 45 mm overhang length, and two flutes10° clearance angle.
- A thin 100 × 100 × 5 mm wall, Ti-6Al-4 V (TC4) alloy, can be seen as one cantilever plate.
- The modal parameters of the tool and the workpiece are shown in Section 4.1.
- The cutting coefficients used for Ti-6Al-4 V for mills are presented in Section 4.2. The specific indentation coefficient K_{sp} is 30,000 N/mm^3.

From the results obtained, how big difference exists between the chatter lobes obtained either considering independent both subsystems or depending on the relative analysis, as shown in Fig. 7. In this figure, the behavior of the tool is represented with circle as an independent entity and the workpiece as an independent entity with a plus sign and the method analyzed above, considering the relative movement, with the solid lines. In addition, the lobes, by using the relative transfer function method, but not including process damping effects, are displayed with squares. It is observed that they are significantly different between the solid lines and squares.

5.1 Experimental verification

Milling experiments are performed to validate the correctness of the model proposed, and analyses of the results are shown in Fig. 8. It can be noticed that at a speed of 2600 rpm, the stability charts indicate very different critical depths b^{p}_{lim}. For each methodology, with regard to a single tool subsystem, the b^{p}_{lim} is 23 mm and for the independent workpiece, the b^{p}_{lim} is 3.2 mm. However, with relative movement proposed, the critical depth b^{p}_{lim} is 4.8 mm, which indicates that 3.2 mm depth that the workpiece imposes will be really a stable situation.

Machining was carried out in these two situations. The point A (2600 rpm, 3.5 mm) of the workpiece surface quality, cutting force, and force spectrum analysis results are provided in Fig. 8a–e, respectively. There is no chatter in the point A.

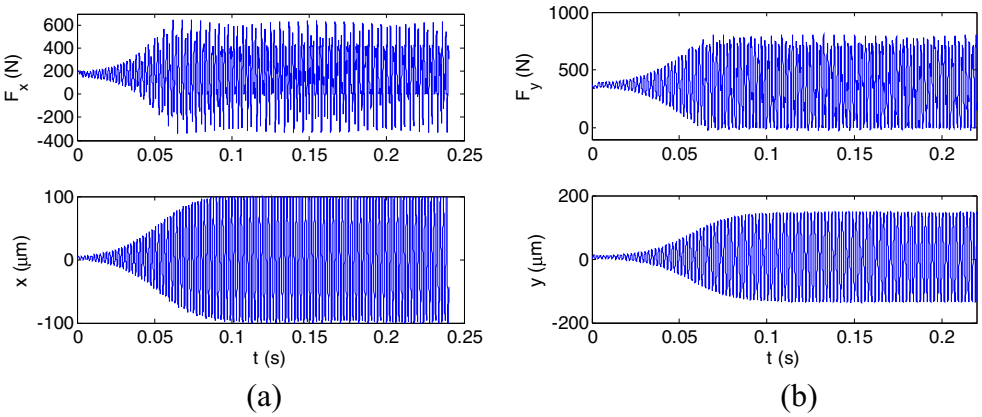

Fig. 10 The *x* and *y* directions of force and displacement of D simulation of the unstable point

Force spectrum shows that the spindle frequency of forced vibration or cutter tooth cutting frequency is about 87 Hz and its integer times. Severe chatter can be observed in the point B (2600 rpm,5.5 mm), which can also be verified by the force spectrum. Chatter occurs at 1072 Hz near the structure first mode of the tool in Fig. 8b–f. From the experimental results, we can get, machining is conducted under this depth (4.8 mm), resulting in a stable milling, which is in accordance with the theoretical prediction.

5.2 Verification of time domain simulation

The time domain simulations are carried out to validate the model considering process damping can predict stability limits at low speed in milling of thin-walled workpiece accurately, comparing with excluding process damping. Both of stability lobes are presented based on the relative transfer functions, as shown in Fig. 7.

For case C (1500 rpm, 4 mm), without consideration of the process damping method, it is located in the stability lobes, which are presented with squares. So the prediction of point C is not stable. However, it is also located below the stability lobes, displayed with the solid lines, which provides a stable result. The time domain simulation corroborates these predictions, consistent with the stability lobes including process damping, as shown in Fig. 9.

Figure 9a, b shows the x and y direction forces and displacements, respectively, for case C. It can be noticed that, basically, there are stable fluctuations in a relatively small region. So the point C is actually supposed to be stable. It is also proved that the influence of process damping is more stable than that without considering damping process.

For case D (1500 rpm, 6 mm), the simulation results are shown as follows below:

From the above results, we can see the expected force and displacement profile. Two kinds of analysis of the chatter stability lobe diagrams with process damping and not considering all show unstable cutting for the point D, which are consistent with time domain simulation. Both x direction and y direction of force and corresponding displacement of fluctuation are great, as shown in Fig. 10a, b, with the occurrence of the chatter.

6 Conclusion

(1) In the paper, the model of considering the process damping is simplified into two degrees of freedom of the mutual vertical elastic damping system of thin-walled workpiece, then one energy-based modeling is carried out to identify process damping coefficient which is then used in stability analysis.

(2) The dynamic model and the critical condition of stability determined by the relative dynamic characteristics between cutter subsystem and thin-walled subsystem are proposed to obtain the reasonable and accurate stability domain.

(3) The model of process damping is integrated into the ZOA method to establish the stability lobes. It can be seen that in the case of low speed, the influence of process damping is considered, and the stable cutting area will increase obviously. And the correctness of the model is verified by experiments and time domain simulation.

(4) Considering the process damping effect in the course of milling, conditions for the generation of chatter besides cutter geometry and each direction frequency response function of structure of thin-walled workpiece and the material properties of the thin-walled workpiece with the cutter speed and depth of cut are closely related.

Acknowledgments This work was supported by (National Natural Science Foundation of China) NSFC 51105072 and 51475087 and supported by Fundamental Research Funds for the Central Universities N150304005 and N140301001 and Education Department of Liaoning Province Key Laboratory Project (LZ2014016).

References

1. Bravo U, Altuzarra O, López de Lacalle LN, Sánchez JA, Campa FJ (2005) Stability limits of milling considering the flexibility of the workpiece and the machine. Int J Mach Tool Manu 45:1669–1680
2. Zhu LD, Li HN, Wang WS (2013) Research on rotary surface topography by orthogonal turn-milling. Int J Adv Manuf Technol 69:2279–2292
3. Wan M, Ma YC, Zhang WH, Yang Y (2015b) Study on the construction mechanism of stability lobes in milling process with multiple modes. Int J Adv Manuf Technol 79:589–603
4. Cao HR, Li B, He ZJ (2012) Chatter stability of milling with speed-varying dynamics of spindles. Int J Mach Tool Manu 52:50–58
5. Wan M, Altintas Y (2014) Mechanics and dynamics of thread milling process. Int J Mach Tool Manu 87:16–26
6. Altintas Y, Eynian M, Onozuka H (2008) Identification of dynamic cutting force coefficients and chatter stability with process damping. CIRP Ann-Manuf Techn 57:371–374
7. Huang CY, Wang J (2007) Mechanistic modeling of process damping in peripheral milling. J Manuf Sci E-T ASME 129:12–20
8. Huang CY, Wang J (2011) Effects of cutting conditions on dynamic cutting factor and process damping in milling. Int J Mach Tool Manu 51(4):320–330
9. Wan M, Zekai MK, Altintas Y (2015a) Mechanics and dynamics of multifunctional tools. J Manuf Sci E-T ASME 137:011019–011011
10. Wan M, Ma YC, Feng J, Zhang WH (2016) Study of static and dynamic ploughing mechanisms by establishing generalized model with static milling forces. Int J Mech Sci 114:120–131
11. Ahmadi K, Ismail F (2010) Experimental investigation of process damping non-linearity in machining chatter. Int J Mach Tool Manu 50:1006–1014
12. Budak E, Tunc LT (2009) A new method for identification and modeling of process damping in machining. J Manuf Sci E-T ASME 131(5):1–10

13. Budak E, Tunc LT (2010) Identification and modeling of process damping in turning and milling using a new approach. CIRP Ann-Manuf Techn 59:403–408
14. Tunc LT, Budak E (2012) Effect of cutting conditions and tool geometry on process damping in machining. Int J Mach Tool Manu 57:10–19
15. Jaydeep MK, Christopher T, Abbas A, Tony LS (2014) Value of information-based experimental design: application to process damping milling. Precis Eng 18:799–808
16. Ahmadi K, Ismail F (2011) Analytical stability lobes including nonlinear process damping effect on machining chatter. Int J Mach Tool Manu 51:296–308
17. Ahmadi K, Ismail F (2012) Stability lobes in milling including process damping and utilizing multi-frequency and semi-discretization methods. Int J Mach Tool Manu 54(5):46–54
18. Dilley DN, Bayly PV, Brian T, Sean G (2005) An analytical study of the effect of process damping on reamer vibrations. J Sound Vib 280:997–1015
19. Jin X, Altintas Y (2013) Chatter stability model of micro-milling with process damping. J Manuf Sci E-T ASME 135(3):031011
20. Moradi H, Movahhedy MR, Vossoughi G (2012) Bifurcation analysis of milling process with tool wear and process damping: regenerative chatter with primary resonance. Nonlinear dynam 70:481–509
21. Moradi H, Vossoughi G, Movahhedy MR (2013) Experimental dynamic modeling of peripheral milling with process damping, structural and cutting force nonlinearities. J Sound Vib 332:4709–4731
22. Ahmadi K, Altintas Y (2014) Identification of machining process damping using output-only modal analysis. J Manuf Sci E-T ASME 136:051017–051011
23. Tunc L, Budak E (2013) Identification and modeling of process damping in milling. J Manuf Sci E-T ASME 135(2):1–12
24. Altintas Y (2012) Manufacturing automation: principles of metal cutting mechanics, machine tool vibrations, and CNC design. Cambridge University, Cambridge